

See discussions, stats, and author profiles for this publication at: <https://www.researchgate.net/publication/308578002>

Absorbed Shear Energy during Solid Particle Impact on Ductile Surface

Article in *Wear* · December 2016

DOI: 10.1016/j.wear.2016.09.021

CITATIONS

7

READS

288

2 authors:



Yaron Ben Ami

Technion - Israel Institute of Technology

11 PUBLICATIONS 77 CITATIONS

SEE PROFILE



Avi Levy

Ben-Gurion University of the Negev

197 PUBLICATIONS 3,286 CITATIONS

SEE PROFILE

Some of the authors of this publication are also working on these related projects:



Erosion and particle breakage in conveying systems [View project](#)



characterization of woody biochar from gasification [View project](#)

Absorbed Shear Energy during Solid Particle Impact on Ductile Surface

Y. Ben Ami*, A. Levy

Department of Mechanical Engineering, Ben-Gurion University of the Negev, PO Box 653, Beer-Sheva 81405, Israel.

* Corresponding author. Fax: +972 86472813; Email address: yaronhab@post.bgu.ac.il (Y. Ben Ami).

Abstract

The shearing action of solid particle during its oblique impact on ductile target material is known to be one of the most dominant mechanisms of material removal in erosion. In this work, the shear energy, which absorbed in the target material, was analyzed using numerical model of rigid ellipsoid particles impact at ductile fully-plastic target. The effect of particle shape, impingement angle, angular velocity and orientation on the extent of the shear energy per unit area was examined. It was noticed that backward rotating particles with a long shape produce very high shear energy at low impingement angles (typically under 30°). The high shear energy is due to scooping mechanism, i.e. the particles rotate backward during the impact and detach with their leading tip facing upwards. This enables larger contact surface, which slides on the eroded face of the target material and thus increase the shear energy. It was noticed that for particles with no initial rotation or initial forward rotation, the scooping mechanism does not take place. Also, particles which are more spherical have less tendency to scoop due to lower moment which is exerted on them during the impact. These findings agree with experimental data, which shows higher erosion rate for backward rotating particles, and offer a reasonable mechanistic cause to this observation. Moreover, the ascent in the shear energy with the particle sharpness and their higher tendency for scooping, present additional explanation for the well-known phenomena of sharp particle which erode more severely than spherical particles.

Keywords: Solid particle impact; Shear energy; Angular velocity; Impingement angle; Particle shape; Particle orientation.

Nomenclature

English Letters

| | | |
|-----------------------------|--|----------------|
| A_m | particle cross section area | m^2 |
| C_μ | damping coefficient | |
| F | force | N |
| $G(x,y)$ | particle surface function in implicit form | |
| $g(x,y)$ | particle Surface function in explicit form | |
| I_p | particle momentum of inertia relative to its center mass in primary coordinate system | $kg \cdot m^2$ |
| $\hat{i}, \hat{j}, \hat{k}$ | body-fixed axes system | |
| $\hat{i}, \hat{j}, \hat{k}$ | inertial axes system | |
| M_{cm} | moment relative to the particle center mass | $N \cdot m$ |
| m_p | particle mass | kg |
| \hat{n} | normal to surface vector | |
| P_d | dynamic hardness | Pa |
| p_m | particle section perimeter | m |
| R_m | particle minor radius | m |
| r, r' | spherical coordinates system radial distance | |
| \vec{r} | location on particle surface relative to its center mass | m |
| S | particle surface area | m^2 |
| \hat{t} | tangent to surface vector | |
| \vec{U} | local particle velocity | m / s |
| W_s'' | shear energy per unit area | J / m^2 |
| \vec{x} | particle location vector | m |
| Y_d | dynamic yield strength | Pa |
| X,Y,Z | body-fixed coordinates | m |
| x,y,z | inertial coordinates | m |

Greek Letters

| | | |
|-----------|---|------------|
| α | particle impingement angle | rad |
| β | particle rake angle | rad |
| β_s | standard rake angle | rad |
| φ | spherical coordinates system polar angle | rad |
| γ | deviation from standard rake angle | rad |
| η | ratio of major to minor ellipsoid axis | |
| μ | ratio of tangential traction to normal pressure | |
| θ | spherical coordinates system azimuth angle | rad |
| ρ_s | Target material density | kg / m^3 |

| | | |
|----------|----------------------------------|----------------|
| τ | <i>shear stress</i> | <i>Pa</i> |
| ω | <i>particle angular velocity</i> | <i>rad / s</i> |
| ψ | <i>particle shape factor</i> | |

Subscripts

| | |
|------|---|
| 0 | <i>initial value</i> |
| cm | <i>value related to the center mass</i> |
| f | <i>value at the end of the impact</i> |
| i | <i>value at the beginning of the impact</i> |
| x | <i>in x direction</i> |
| y | <i>in y direction</i> |
| z | <i>in z direction</i> |

1. Introduction

Erosive wear by solid particles impact is a complex problem involving the collision of shaped particles on a surface with various impact angles, velocities and orientations. In order to understand the material removal process at particle impact, an approach of single rigid particle impact against a deformable target material is commonly used.

The impact process of rigid particle against ductile target materials have been the subject of many studies. Finnie [1] was the first to suggest a model for the volume of the crater produced at impact by solving the momentum equations of the particle assuming only plastic behavior of the target. Finnie [1] assumed constant ratio of horizontal to vertical force which the target exerting on the particle, thus was able to receive analytical solution. Rickerby & Macmillan [2] extended this model to account for the change of the resistive surface area of the target for spherical particles and Hutchings [3] done the same for square plates. The change of the resistive area causes the momentum differential equations to be non-linear, hence had to be solved numerically. Sundararajan & Shewmon [4][5] improved the model for spherical particles to account for the behavior of different target materials and received the indentation size as well as the rebound parameters of the particle and the absorbed kinetic energy. Papini & Spelt [6][7] extended the analysis for arbitrary shape particles, but solved only for rhomboid particles with different tip angles. All of these studies mentioned above used the assumption of fully-plastic behavior with no fracture mechanics included, however managed to receive good agreement with experiments. Some recent works [8][9][10][11] used finite elements methods in order to simulate the impact.

In these works a constitutive model for the stress-strain (such as Johnson & Cook [12]) is adopted as well as fracture criterion [13]. A further improvement, enabled with the ascent of computational power, is the smoothed-particle-hydrodynamics method [14][15], a mesh free method, which was used in order to overcome difficulties such as large strains which distort the computational grid. These recent works accuracy is larger comparing to the fully-plastic, no fracture simulations and they are also able to account for real chipping process by abrasive particle. Nevertheless, as will be shown in this work, a rather simple model for the solid particle impact, embracing the assumption of fully plastic, no fracture behavior, can perform very well at predicting the crater volume and energy absorption during smooth particle (no angular tips) impact. This model is able to explain some experimental observations regarding the effect of particle angular rotation and particle shape on erosive wear.

There are several dynamic parameters that are known to affect the wear rate at solid particle impact: the effects of impact velocity [16][17][18][20] and impact angle [1][20][21][22] were investigated extensively. However, the effect of particle shape and particle angular velocity is much lesser understood. Finnie et al. [17] related the angular velocity to increasing in the velocity exponent. Deng et al. [24] studied the effect of particle rotation and described the phenomenon of increased wear when the particle impacts with backward rotation. Hutchings [3], when studied square plates, also find that particles which attain backward rotation during the impact cause more material removal. The effect of particle shape was investigated widely [10][25][26][27] and the general conclusion is that sharp particles erosion is more severe. Some explanations were given for the particle sharpness effect on the erosion extent, such as enhanced strains and micromachining mechanism. However, in this study the effect of the particle shape on the shearing action is examined. In order to study the effect of these parameters on the extent of erosion, we have to define the parameters that represent best the probability of material removal. The volume of the indentation produced by the particle cannot be connected directly to the extent of material removal due to pile up of the compressed material in form of indentation lips, which are not removed in the first impact, as was shown in the work of Hutchings & Winter [28], Levy [29] and Sundararajan & Shewmon [4]. However, material removal depends largely on the shearing action of the particle. According to Sundararajan [30] and Winter & Hutchings[31], the frictional forces between the particle and the target material introduce very high shear strain in the near surface region of the eroded material, which leads to highly deformed lip formation. In

this region localization of the shear strains causing formation of adiabatic shear bands, which are dominant failure mechanism in ductile materials [31][32]. Therefore, the parameter, which was chosen as representative, is absorbed shear energy per unit area. This parameter will be calculated using numerical particle impact model. In this work, a simple fully-plastic, no fracture model for the impact of rigid particle with ductile surface is developed. The model extends the aforementioned works [2]-[7] in its ability to calculate absorbed shear energy rather than total energy for any given arbitrary 3-dimensional particle shape, with an improved algorithm for calculating the time variant contact area. Additionally, a modified equation for calculating the shear force in dependence of the sliding velocity is presented, which yields good agreement with absorbed energy experimental data.

2. Model description

2.1. Particle definition

The particle is an entity defined by 5 parameters:

- Center mass location- \vec{x}_{cm}
- Center mass velocity- \vec{U}_{cm}
- Particle attached coordinate system $\hat{I}, \hat{J}, \hat{K}$ (defines the orientation)
- Particle angular velocity - $\vec{\omega}$. Defining the rate of change of the Particle attached coordinate system.
- Surface function relative to the center mass, given in the particle attached $\hat{I}, \hat{J}, \hat{K}$ coordinate system (defines the shape- sphere, ellipsoid, paraboloid, cube, etc.): $z = g(x, y)$

2.2. Target surface definition

The surface is defined by an array of nodes. Each node has its own (x, y, z) position, which can be changed between the time steps. The surface is initialized with $x \in [0, \text{SURFACE LENGTH}]$, $y \in [0, \text{SURFACE LENGTH}]$, $z = 0$ for rectangular flat surface.

2.3. Forces and moments calculation

There are few distinct regimes on which the impact can take place: elastic, elasto-plastic, fully-plastic and hydrodynamics. The regime of the impact can be evaluated through the non-dimensional number suggested by Johnson [33]: $\rho_s U_0^2 / Y_d$, where ρ_s is the target density, U_0 is the impact velocity and Y_d is the dynamic yield strength of the target, correlates to the dynamic flow pressure by $P_d \approx 3Y_d$ [34]. This number can be interpreted as the ratio of the ‘stagnation pressure’ of the moving projectile, conceived as a fluid jet, to the strength of the target material. When this number is about 10, the inertia of the target material becomes more dominant than its hardness, hence the material start to receive a fluid like behavior. Johnson [33] remarked that when the number $\rho_s U_0^2 / Y_d < 1 \times 10^{-6}$, the collision is fully elastic and when $\rho_s U_0^2 / Y_d > 1 \times 10^{-3}$, the elastic zone is much smaller than the plastic zone, hence the collision can be treated as fully plastic.

In the current model the fully plastic collision is assumed (justification for this assumption will be presented later on by calculating the value of $\rho_s U_0^2 / Y_d$). Together with the Amonton’s law, relating the tangential traction to the normal pressure, we write the force exerted on the particle:

$$\vec{F} = -P_d \int_S (\hat{n} + \mu \hat{t}) dS \quad (1)$$

The moment relative to the particle center mass is:

$$\vec{M}_{cm} = \int_S \vec{r} \times \vec{F} dS \quad (2)$$

where, $P_d [MPa]$ is the dynamic hardness of the material, which typically larger than the static hardness of the material by a factor of $\sim 1 \div 2$ [4][34] which relates to the strain rate hardening. The value of P_d is calibrated from normal impact experiments. μ is friction coefficient, satisfies the assumption $\tau = \mu P$, where τ is the shear stress. \hat{n} is a unit vector normal to the particle surface in the outward direction, \hat{t} is a unit vector tangent to the particle surface in the direction of the velocity in the specific point (not necessarily the center mass velocity, due to particle rotation).

The value of μ is assumed to depend on the local sliding velocity magnitude [5][35]. Sundararajan [5] calculated μ based on measured energy absorption during particle impact. He showed that using constant μ yields major error in predicting the absorbed kinetic energy and that μ depends greatly on the sliding velocity. The calculation of Sundararajan [5] showed that μ exhibit a general trend of rising together with the sliding velocity in the range of $U_t = 50 \div 100 \text{ m/s}$. At larger velocities, μ presented constant or slightly descending trend as a function of sliding velocity. This is contradictory to the case of sliding friction, which is reduced with increasing of the sliding velocity. In the case of sliding friction, the temperature may rise in the near surface region thus cause local region of surface softening which reduces the adhesion traction. However, for particle impact the case is of adiabatic shear [31][32], i.e. the shear strain rate is very high and the strains are highly localized, which can cause strain rate hardening. In general, both mechanisms exist and μ should be affected by both adhesive friction and plastic shear friction. However, according to Sundararajan [5] results, it seems that the shear strain rate hardening is dominant in the examined range of impact velocities. Hence, based on Sundararajan [5] finding and for simplicity we assumed that μ is rising linearly with the sliding velocity:

$$\mu = C_\mu \cdot |U_t| \quad (3)$$

where C_μ is the ‘damping’ coefficient of the material, which can be related to the material strain rate hardening, thermal diffusion and the measure of localization of strains in the material. This parameter should be calibrated from experiments. Worth noting that the linearly ascending assumption is a simplification of the problem. A more general model should account for effects such as thermal softening and adhesive friction.

The local sliding velocity is calculated by:

$$U_t = (\vec{U}_{cm} + \vec{\omega} \times \vec{r}) \cdot \hat{t} \quad (4)$$

Where \vec{U}_{cm} is the particle center mass velocity, \vec{r} is the radius vector between the center mass to a surface point and $\vec{\omega}$ is the particle angular velocity.

The normal to the surface on each particle point is defined by the gradient of $G(x, y, z)$, where:

$$G(x, y, z) = g(x, y) - z = 0$$

$$\hat{n} = \frac{\vec{\nabla} G(x, y, z)}{|\vec{\nabla} G(x, y, z)|} \quad (5)$$

The tangent to the surface in the direction of the velocity is the projection of \vec{U} on a plane with normal \hat{n} :

$$\hat{t} = \frac{\vec{U} - \vec{U} \cdot \hat{n}}{|\vec{U} - \vec{U} \cdot \hat{n}|} \quad (6)$$

The method which was chosen to integrate the contact surface of the particle is discretization of the particle surface by the target surface nodes. Using small enough time step, the deformed surface is parallel to the particle surface. The limits of integration are defined by the nodes of the target which are in contact ('active'). The active nodes can be found by using spherical coordinate system for describing the particle function and the target nodes:

$$\begin{aligned} r' &= \sqrt{x^2 + y^2 + z^2} \\ \theta' &= \cos^{-1}(z / r') \\ \varphi' &= \tan^{-1}(y / x) \end{aligned} \quad (7)$$

where the prime superscript denotes coordinates of the surface nodes. All of the target nodes are described in the spherical system and then each node φ', θ' is used to calculate r , the projection of the node on the particle surface, by using the particle surface function:

$$z = g(x, y) \Rightarrow r = \tilde{g}(\varphi', \theta').$$

If, for a certain node, $r' \leq r$, meaning the surface node is inside the particle, this point is active, i.e. exert force and should be included in the integration. This method is presented schematically in Fig. 1. Here, a particle with an impact velocity, U_0 , impingement angle, α , and impact orientation angle, β , impact a horizontal surface. Once each projection of target nodes on the particle surface is calculated, the discrete area of each projected node can be calculated by the equation:

$$dS = \sqrt{1 + \left(\frac{\partial g(x, y)}{\partial x} \right)^2 + \left(\frac{\partial g(x, y)}{\partial y} \right)^2} dA_{xy} \quad (8)$$

where, dA_{XY} is the area of the projection of the node on the particle XY plane.

At each time step, the active (in contact) surface points are updated to their projection on the particle surface:

$$(r', \theta', \varphi')_{t=m} \Rightarrow (r, \theta, \varphi)_{t=m+1}$$

This method for identifying and updating the surface nodes presents improvement over the models in [2]-[7]: Changing of particle shape can be done very easily by changing the particle surface function and does not involve modification of the calculation algorithm. Even though the particle can be of arbitrary shape, the representation of the particle as an analytical entity, which does not composed of computational nodes, is computational effective.

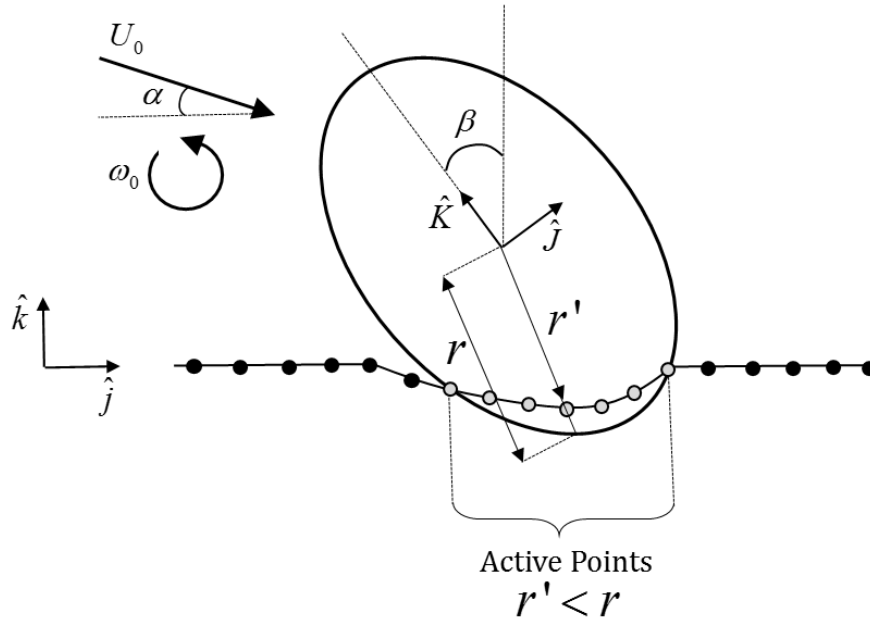


Fig. 1. Illustration of the particle and the surface nodes interaction.

2.4. Particle's equations of motion

Translational momentum:

$$\begin{cases} \frac{d\vec{U}_{cm}}{dt} = \frac{\vec{F}}{m_p} \\ \frac{d\vec{x}_{cm}}{dt} = \vec{U}_{cm} \end{cases} \quad (9)$$

Angular momentum relative to the particle center mass:

$$[I_p] \frac{d\vec{\omega}}{dt} + \vec{\omega} \times [I_p] \vec{\omega} = \vec{M}_{cm} \quad (10)$$

Where $[I_p]$ is calculated relative to the center mass in the primary coordinate system $(\hat{I}, \hat{J}, \hat{K})$, hence the term $\vec{\omega} \times [I_p] \vec{\omega}$, which allows $[I_p]$ to remain constant, when $(\hat{I}, \hat{J}, \hat{K})$ changes in time.

For primary coordinates system (I_p is diagonal), these equations receive the Euler form:

$$\begin{cases} M_x = I_{xx} \frac{d\omega_x}{dt} + (I_{zz} - I_{yy}) \omega_y \omega_z \\ M_y = I_{yy} \frac{d\omega_y}{dt} + (I_{xx} - I_{zz}) \omega_x \omega_z \\ M_z = I_{zz} \frac{d\omega_z}{dt} + (I_{yy} - I_{xx}) \omega_x \omega_y \end{cases} \quad (11)$$

Then, the direction of the axis of the particle attached system is defined by:

$$\begin{cases} \frac{d\hat{I}}{dt} = \vec{\omega} \times \hat{I} \\ \frac{d\hat{J}}{dt} = \vec{\omega} \times \hat{J} \\ \frac{d\hat{K}}{dt} = \vec{\omega} \times \hat{K} \end{cases} \quad (12)$$

2.5. Solver

Due to linearity of the translational motion equations, the particle's center mass velocity and location (Eq.(9)) is solved directly for each time step using first order explicit scheme. The non-linear equation of angular motion (Eq. (11)) and the particle attached axis equations (Eq. (12)) are solved by 4th order Runge-Kutta method.

3. Model validation

The model was validated against experimental data of Sundararajan & Shewmon [4][5], where they conducted impact experiments of hard steel ball of 4.76 mm diameter against ductile target material (copper, brass and stainless steel) and measured the indentation volume and kinetic energy loss of the ball. In this study we used the materials properties of P_d found by Sundararajan & Shewmon [4][5] and calibrated the value of the damping coefficient C_μ by the value which gave the best fit to the absorbed energy in the experiments. The target materials properties are listed in Table 1. The predicted values of the volume removal against experimental data are given in Fig. 2, where the volume removal was calculated at the end of the impact by numerical integration of the indentation depth:

$$V_{ind} = \left| \iint_{A_{ind}} z \cdot dx dy \right| \quad (13)$$

where, the integration is over nodes where $z < 0$.

The independent variables in Fig. 2 are: (i) Impact velocity magnitude, U_0 , defined as the particle velocity magnitude at the beginning of the impact. (ii) Impingement angle, α , defined as the angle between the particle velocity vector and its projection on the surface at the beginning of the impact (for illustration, see Fig. 1).

Calculation of $\rho_s U_0^2 / Y_d$ for the range of impact velocities, using the relation $P_d \approx 3Y_d$, yields values of 0.06÷0.8 for copper, 0.05÷0.6 for brass and 0.01÷0.2 for SS301. Note that for the entire range of velocities the value of $\rho_s U_0^2 / Y_d$ is well over 0.001 and below 10, thus the fully-plastic, no hydrodynamic behavior assumption is justified.

Table 1. Target Materials Properties

| Target Material | P_d [MPa] | $C_\mu \times 10^{-3}$ |
|---------------------|-------------|------------------------|
| Copper | 1100 | 2.5 |
| Brass | 1350 | 2.22 |
| Stainless Steel 301 | 4100 | 0.55 |

Fig. 2 presents very good match between the experimental data and the model prediction of the indentation volume for spherical particle. Since the new developed model can be adjusted to simulate non-spherical particle impact by only changing the particle surface definition: $z = g(x, y)$ it can be argued that the model is valid for these cases too.

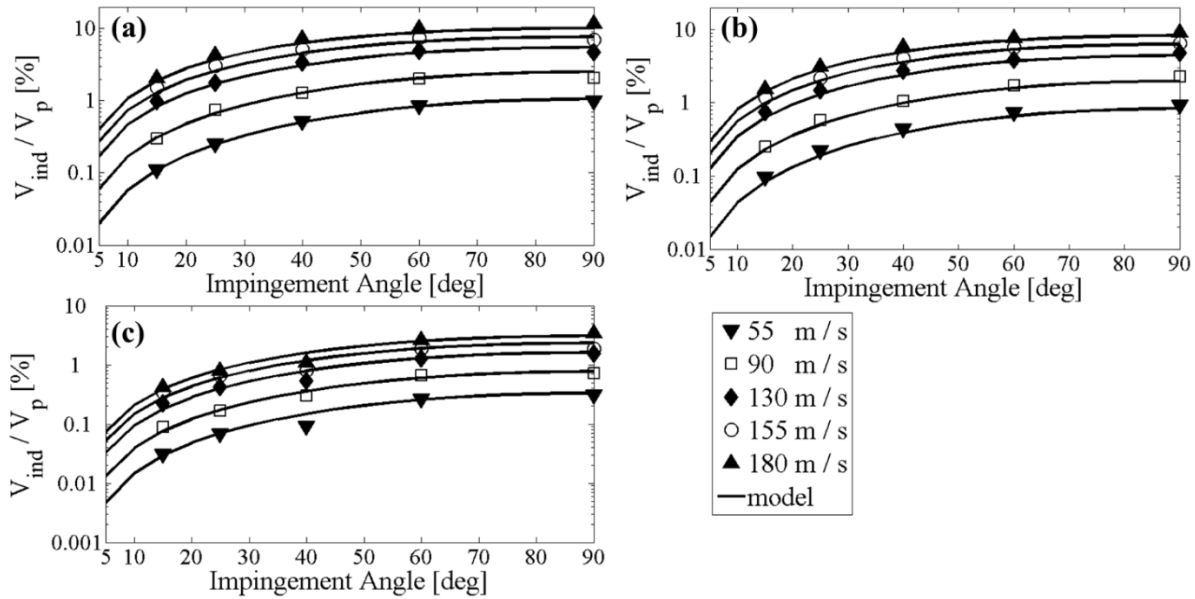


Fig. 2. Ratio of indentation volume to particle volume versus the impingement angle for different impact velocities. Model results versus Sundararajan & Shewmon [4] experimental data. Target material is (a) copper, (b) brass and (c) ss301.

The values of model prediction for absorbed translational kinetic energy against experimental data of Sundararajan [5] (rotational energy was not measured) is given in Fig. 3. We can notice that the absorbed energy is predicted less accurately than the volume removal. This is due to many factors affecting this parameter, such as heating of the particle and the surface and cracks

initiation. The measurement of the kinetic energy loss is somehow less accurate than the volume removal too, due to the difficulty of measuring the velocity of the particle in the exact detachment moment. Nevertheless, the results of the model are in good agreement with the experiments and the trends are very much alike.

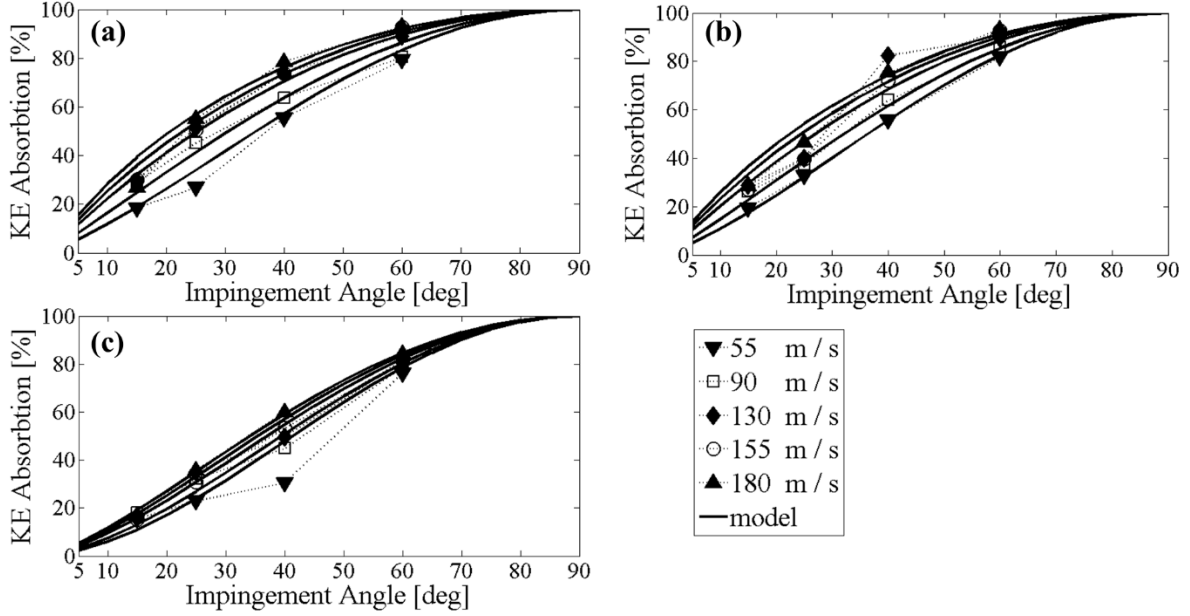


Fig. 3. Absorbed particle energy versus the impingement angle for different impact velocities. Model results versus Sundararajan [5] experimental data. Target material is (a) copper, (b) brass and (c) ss301.

4. Numerical Simulations of non-spherical particles

The shape of abrasive particle is usually a complex not symmetric shape with sharp corners. The effect of the sharp corners was studied by Hutchings [3] and Papini & Spelt [7], by conducting simulations and experiments of square plate impact. In this work, we examine the effect of the shape of smooth particle. In order to do so, the particles are 3-dimensional prolate ellipsoids with a pair of equal axes, as presented in Fig. 4. This shape allows changing its sphericity by changing the magnitude of the primary axis. The surface equation for ellipsoid particle:

$$Z^2 = \eta^2 \left[R_m^2 - (X^2 + Y^2) \right] \quad (14)$$

where R_m is the particle minor radius and η is the ratio of particle major radius to minor radius.

X, Y, Z are given in the body fixed coordinates $(\hat{I}, \hat{J}, \hat{K})$, which can be written in spherical coordinates:

$$r^2 = \frac{\eta^2 R_m^2}{\eta^2 \sin^2 \theta + \cos^2 \theta} \quad (15)$$

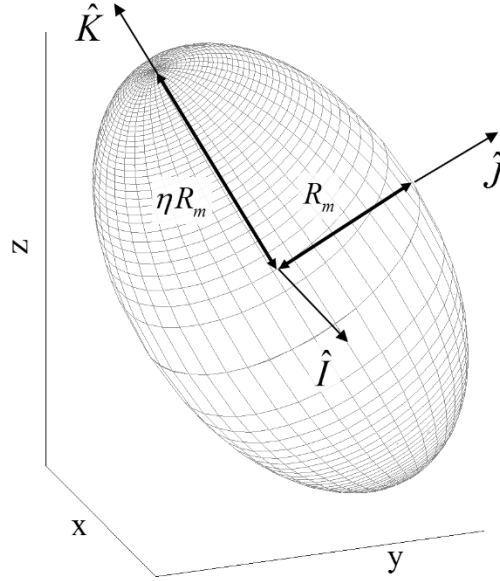


Fig. 4. Prolate ellipsoid particle and its body-fixed coordinate system.

The unit surface normal vector:

$$\hat{n} = \frac{1}{\sqrt{\eta^4 \sin^2 \theta + \cos^2 \theta}} (\eta^2 \sin \theta \cos \varphi \hat{I} + \eta^2 \sin \theta \sin \varphi \hat{J} + \cos \theta \hat{K}) \quad (16)$$

The discrete surface area:

$$dS = \sqrt{1 + \eta^4 \tan^2 \theta} dX dY \quad (17)$$

The sphericity for axisymmetric particles is proportional to their circularity and it is calculated by:

$$\psi = \frac{4\pi A_m}{p_m^2} = \frac{8\eta}{4(\eta^2 + 1) - (\eta - 1)^2} \quad (18)$$

where A_m is particle section orthogonal to minor axis (\hat{I} or \hat{J}) and p_m is this section perimeter.

The particles shape factors which were used in the simulations are $\eta = 1$ (sphere), 1.7, 2.25 and 2.75 which correspond to $\psi = 1$ (sphere), 0.9, 0.8 and 0.7 respectively.

5. Shear Energy of Abrasive Particle

As was mentioned in the introduction, the examined parameter is the absorbed shear energy per unit area. The shear energy is calculated as integration of the force which is tangent to the surface (\vec{F}_s) through the entire contact interval. Then, the shear energy per unit area (W_s) is the division of the total shear energy by the final indentation surface area:

$$\vec{F}_s = \mu P \int_S \hat{t} dS \quad (19)$$

$$W_s = \frac{\int_S (\vec{F}_s \cdot \vec{U}) dt}{\int_S dS} \quad (20)$$

6. Simulation Setup

Ellipsoid steel particle of minor radius $R_m = 2.38 \text{ mm}$ and density 7800 kg/m^3 was simulated. The target material was brass $P_d = 1350 \text{ MPa}$, $C_\mu = 2.22 \times 10^{-3}$. The initial translational velocity was set to $U_0 = 100 \text{ m/s}$ in impingement angle α relative to the plane:

$$\vec{U}_{cm,0} = U_0 (\cos \alpha \hat{j} - \sin \alpha \hat{k}) \quad (21)$$

Three cases of initial angular velocity were examined: non angular velocity, positive angular velocity (in \hat{I} direction, i.e. “backward rotation”) and negative angular velocity (in $-\hat{I}$ direction, i.e. “forward rotation”). The angular velocity was set to correspond to minimum particle tangential velocity which is 10% of the center mass initial velocity: $|\omega_0| = 0.1 U_0 / R_m$. This gave value of $|\omega_0| \approx 670 \text{ rev/s}$. In order to avoid complications of changing the particle orientation

when changing the initial angular velocity, the angular velocity of the particle was initiated in first time step of the impact. The orientation of the particle in the moment of impact, which can be described by the rake angle β (defined as the angle between the particle major axis (\hat{K}) and the normal to the target surface (\hat{k}), see Fig. 1), was set at first to be: $\beta = 90^\circ - \alpha$ (will be denoted as standard rake angle β_s), where α is the impingement angle. The last section of the results (7.2) examines the effect of deviation from the orientation from the standard rake angle (denoted γ , where $\gamma = \beta - \beta_s$).

The number of target surface computational nodes in the simulations was 640,000 (approximately 640 nodes per particle diameter) and the time step was set to 1×10^{-7} s. These values proved to yield consistent values for the examined parameters.

7. Results and Discussion

7.1. *Standard Rake Angle*

The shear energy per unit area produced by the abrasive particle is presented in Fig. 5 for the different particle shape factors. The most outstanding feature which can be noticed in Fig. 5(a) and Fig. 5(b) is the peak occurs at low impingement angles for the sharp particles ($\psi = 0.7, 0.8$) with initial backward rotation. For shape factors of $\psi = 0.9, 1$ this peak does not occur and the trends of all angular velocity cases are the same. In order to understand the nature of this major ascend in the shear energy we can examine the particle final orientation relative to its initial orientation. To illustrate this parameter in a clear way we choose to present the change of the body-fixed \hat{K} axis, which is in the direction of the ellipsoid major axis. Due to symmetry of the problem, the particle rotation is in yz plane, hence the change of the particle orientation can be simply defined by the change in the y or z component of \hat{K} . The relative change of particle between its initial and final orientation is depicted by the $K_{z,f} / K_{z,i}$ (K_z is the cosine of the angle between the particle attached \hat{K} to the global \hat{k} axis). When this ratio is smaller than 1 and larger than zero, the particle exit angle is smaller than the impingement angle. When the ratio is smaller than 0, the particle perform a scooping action, i.e. its leading tip faces upward at the end of the impact. The different cases are illustrated in Fig. 6.

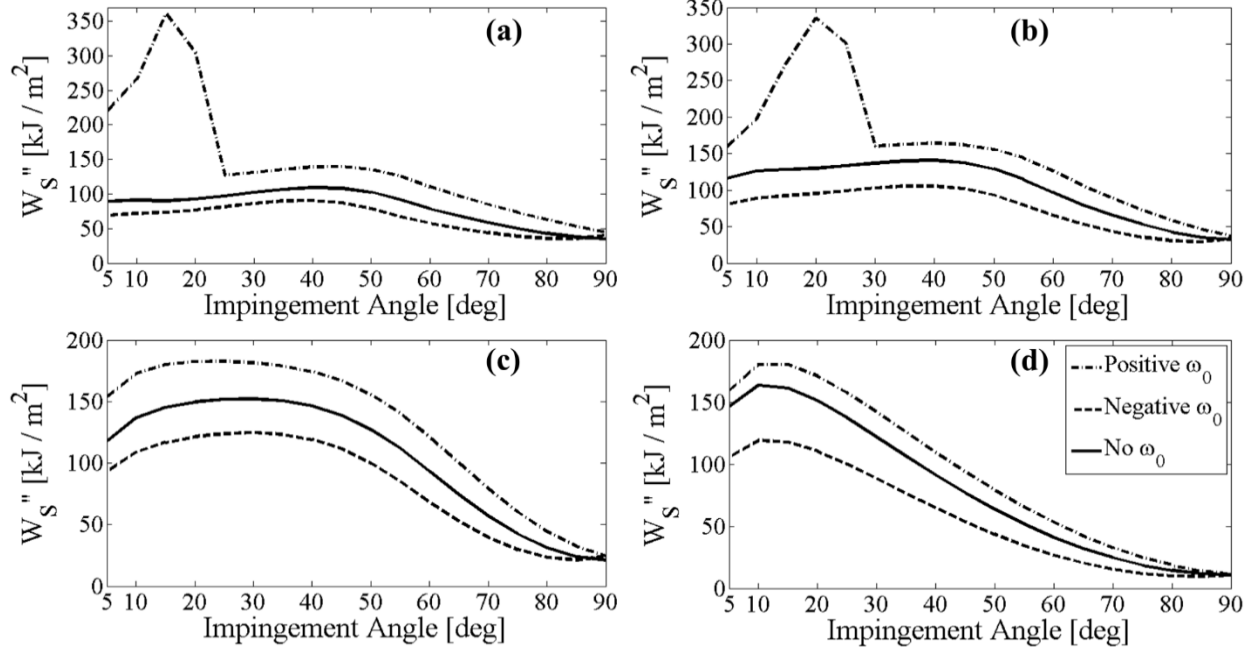


Fig. 5. Shear energy per unit area versus the impingement angle for different particle initial angular velocities. Impact orientation angle $\gamma=0^\circ$. Particle shape factor: (a) $\psi=0.7$, (b) $\psi=0.8$, (c) $\psi=0.9$, (d) $\psi=1$.

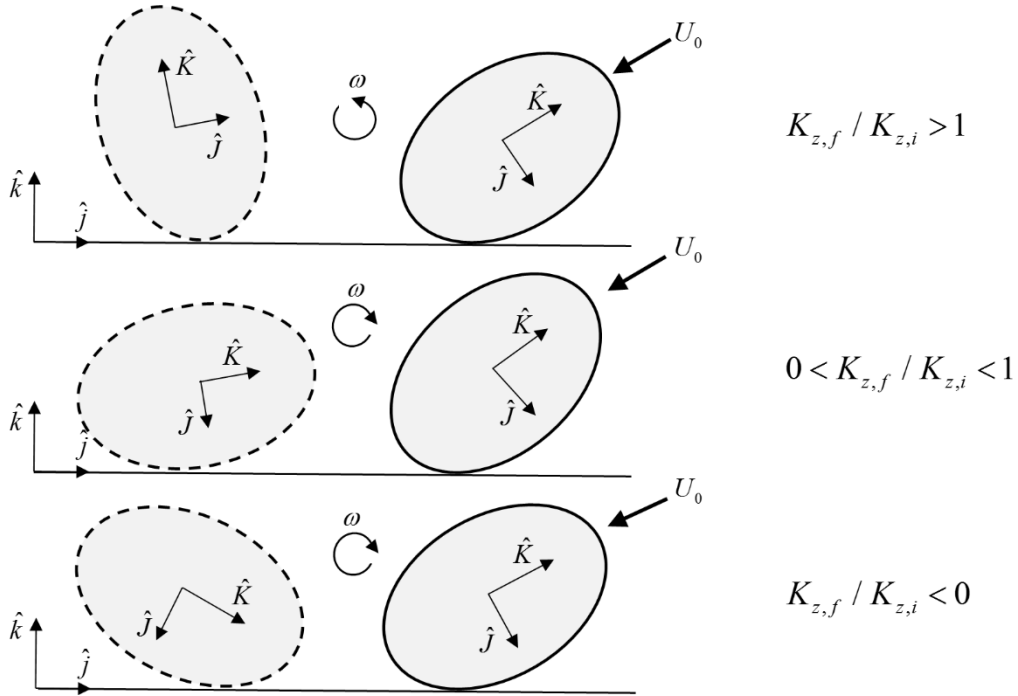


Fig. 6. Illustration of the change in the particle orientation.

Examples for scooping and not scooping particles are presented in Fig. 7. Fig. 7(a) presents the change of the particle orientation during the impact for long shaped particle ($\psi = 0.8$) which produce scooping action ($\alpha = 15^\circ$, $\omega_0 > 0$). The contribution of the scooping action to the shear energy can be seen in the final orientation where the rear part of the particle shears the surface during the particle upward movement. In Fig. 7(b) the particle shape factor is $\psi = 0.9$ and it impacts in the same conditions as in Fig. 7(a). The scooping action does not occur in that case, where the particle still face downwards when it detached.

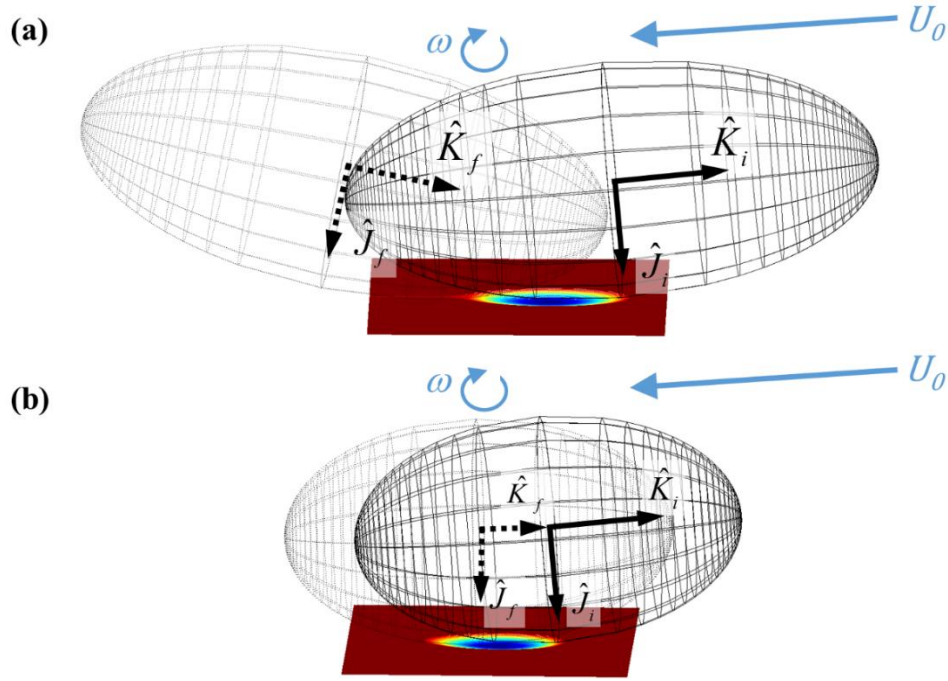


Fig. 7. Change of the particle orientation during the impact and the final form of indentation. Impingement angle is $\alpha=15^\circ$. Particle initialized with backward rotation $\omega_0 > 0$. Colors represent the depth (z) of the indentation. Particle shape factor is (a) $\psi=0.8$ and (b) $\psi=0.9$.

When the particle scoops the surface, a typical narrow crater with a sharp front is formed, while when scooping does not take place, a more rounded crater is formed. This can be shown in Fig. 8, where the crater profile, formed by backward and forward rotating particles, is presented. The sharp front of the crater profile, produced by scooping particles (Fig. 8(a),(b)), is the outcome of the reduction in the contact surface when the particle moves upward while shearing the surface

with its rear part. This phenomena of different crater shape produced by scooping particles will also be presented in section 7.2, discussing the effect of particle initial orientation.

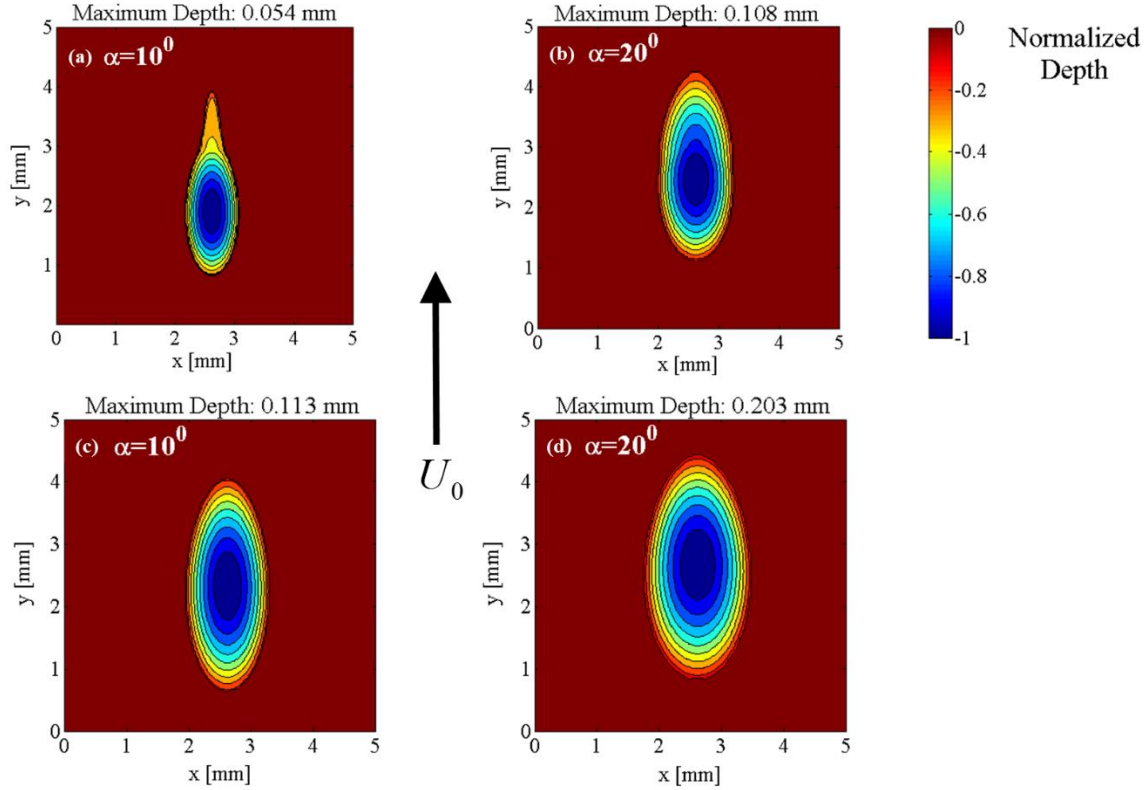


Fig. 8. Crater depth contours for the case of (a,b) backward rotation $\omega_0 > 0$ and (c,d) forward rotation $\omega_0 < 0$. Particle shape factor is $\psi=0.8$ and the impingement angle is (a,c) 10° , (b,d) 20° . Colors represent the normalized depth $z/|z_{max}|$ of the indentation.

Fig. 9 presents $K_{z,f} / K_{z,i}$ as a function of the impingement angle and the initial angular velocity for the different shape factors. We can notice by comparing Fig. 9(a), Fig. 9(b) to Fig. 5(a), Fig. 5(b) ($\psi = 0.7, 0.8$) that there is a clear correlation between the range of impingement angles that produce high shear energy to the range where $K_{z,f} / K_{z,i} < 0$. Thus, we can conclude that scooping action of the particle is the mechanism that produce high shear energy. The high shear energy results from the rotation of the particle inside the target material, which enlarge the surface area of the particle, which is in contact with the target surface. The scooping mechanism operate only in small impingement angles due to the fact that for larger angles, the particle leading tip penetration is large, creating short and deep indentation, which does not allow the rear part of the

particle to plough through the surface. In Fig. 9(c) and Fig. 9(d) ($\psi = 0.9$ and 1), $K_{z,f} / K_{z,i}$ is always larger than 0, i.e. no scooping occurs. Hence, we can conclude that scooping mechanism is possible only for long particles, where the normal force, which operate on the bottom surface of the particle, can produce large enough moment to enable the particle to complete its rotation. For more spherical particles, the arm of the normal force to the center mass is smaller (zero for spherical particles), hence the particle rotation is lesser.

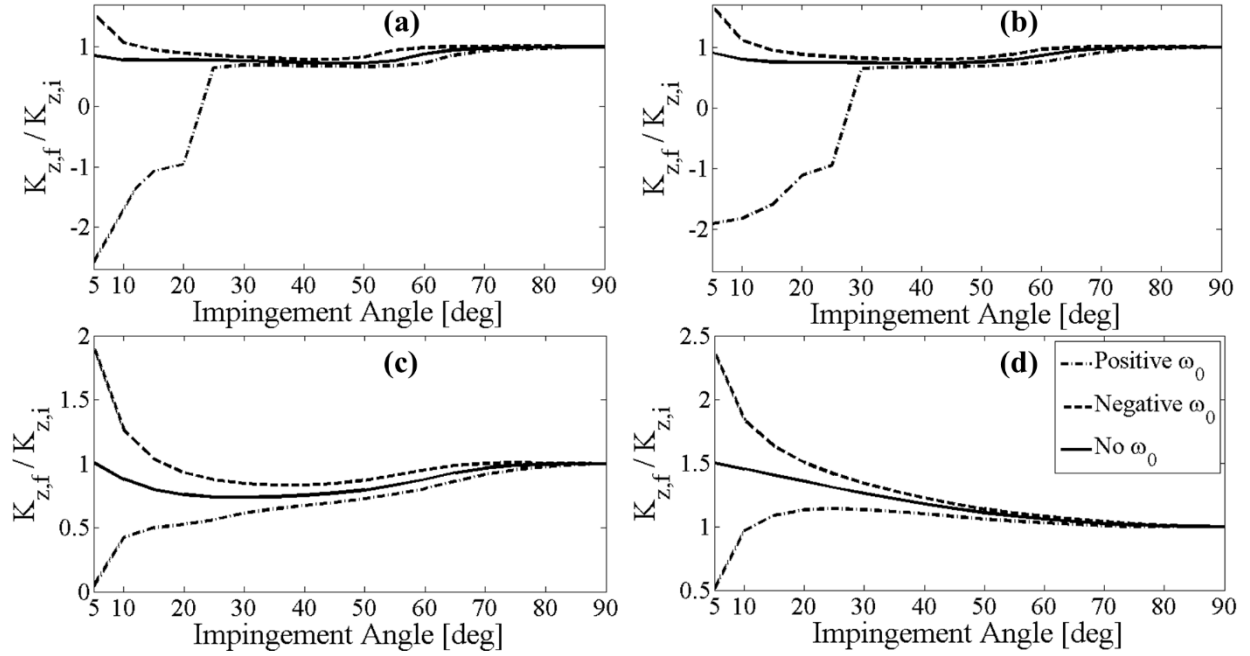


Fig. 9. Final and initial orientation ratio versus the impingement angle for different particle initial angular velocities. Impact orientation angle $\gamma=0^\circ$. Particle shape factor: (a) $\psi=0.7$, (b) $\psi=0.8$, (c) $\psi=0.9$, (d) $\psi=1$.

For most impact angles of no spherical particles, the particle attains positive angular velocity during the impact, regardless of its initial rotation. This can be seen by the smaller than 1 values of $K_{z,f} / K_{z,i}$. This finding is contradictory to the study of Hutchings [3] on impact of angular plates. Hutchings [3] showed that positive angular velocity (backward spin) is only possible on a narrow range of rake angles. Nevertheless, the use of square plates which impact with their angular tip is different from the situation in our simulations. For ellipsoid particles, the particle collides the surface with its bottom front surface, then the moment which exerted is positive. For square plates, the force which acts on the front of the plate is the dominant force, which cause

negative moment. To our understanding, for real arbitrary shaped particles, the situation is closer to the case in our study because the probability of the particle to impact with its bottom surface is much larger than the probability of impact with one of its angular tips.

For all shape factors, in the impingement angles range where scooping does not occur, all angular velocities exhibit the same trend. Nevertheless, positive initial angular velocity produced higher shear energy per unit area. This is because particles with negative initial angular velocity creates deeper indentations. For non-spherical particles, forward rotation deflects their front tip in the direction of the surface. This enables the particle to penetrate deeper due to smaller contact area and consequently a deeper crater is received (see Fig. 8). However, the moment which is exerted on the particle is positive, causing decay of the negative angular rotation. Therefore, due to its lower rotation rate, most of the force which it applies on the target surface is compressive rather than shearing force. Particles with backward rotation are also subjected to positive moment which enhance their rotation rate which cause them to exert large shear force. Deng et al. [24] reported that particles with initial backward rotation creates high lips of deformed material at the edge of the indentation, which suitable to particles performing scooping action. For spherical particles, Deng et al. [25] found that the erosion rate is much less affected by the initial rotation direction than for angular particles. This finding agrees with our results that scooping mechanism does not take place at spherical particles impact. This support the conclusion that high shear energy per unit area, which produced in scooping mechanism, is a dominant factor in the erosion process by solid particles impact.

7.2. Effect of Initial Orientation

In section 7.1, the effect of particle shape and initial rotation was studied for particles that impacts in standard rake angle ($\beta_s = 90^\circ - \alpha$). For the real case, the particles can impact the surface in different orientations independent of the impingement angle. In order to examine the erosion process for more realistic case, the rake angle was deviated from β_s for a given impingement angle. The shear energy per unit area as a function of this deviation (denoted by $\gamma = \beta - \beta_s$) is presented in Fig. 10 for several impingement angles in the case of initial positive angular velocity (backward rotation). When the initial orientation of the particle becomes more “flat” ($\gamma > 0$) we notice the scooping mechanism (by the typical large ascent in the shear energy) for the sharper particles ($\psi = 0.7, 0.8$, Fig. 10(a),(b)). This result is foreseeable because the

effective impingement angle becomes smaller when γ is positive, hence the positive moment which is exerted by the normal force at the particle bottom gets larger and enables the scooping mechanism. The larger the impingement angle is, the larger γ required for scooping mechanism to exist. We can notice some threshold value for γ in dependence of α , above it the scooping mechanism takes place. Then, when increasing γ more, the shear energy decreased as a result of the contact location that approaches to the center of the particle when γ approaches α (completely horizontal particle), which reduces the positive moment on the particle.

The results in Fig. 10 show that scooping mechanism can take place even at intermediate impact angles (up to 40°) if the orientation angle is suitable. This show that particles scooping is not restricted only to very low impingement angles.

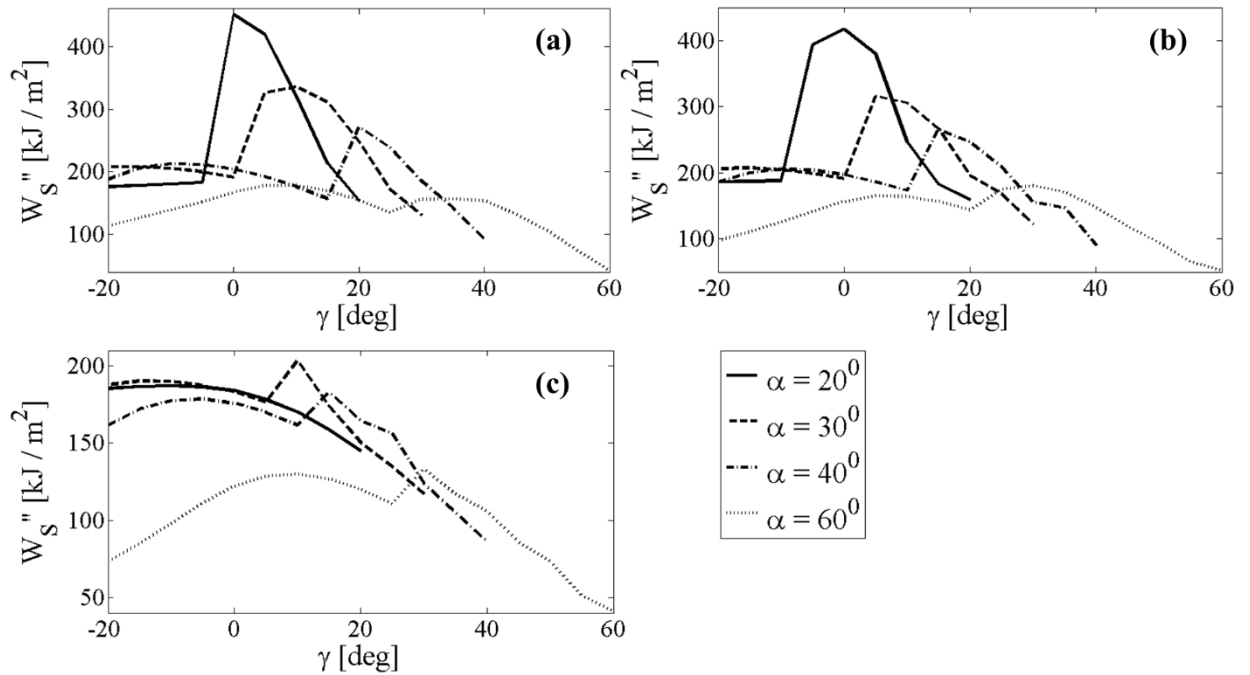


Fig. 10. Shear energy per unit area versus the deviation from the standard rake angle for different impingement angles. The initial angular rotation $\omega_0 > 0$. Particle shape factor: (a) $\psi = 0.7$, (b) $\psi = 0.8$, (c) $\psi = 0.9$.

For blunt particle $\psi = 0.9$ (Fig. 10(c)), only a small increase in the shear energy is seen in the range of γ which enables the scooping mechanism. The contribution of the scooping mechanism

at this shape factor is diminished because the scooping is done only with the front tip of the particle, instead of with its entire bottom surface. Hence, the contact surface is rather small comparing to the sharper particles.

The effect of the orientation angle on the crater shape formed by sharp particle is presented in Fig. 11. When the particle impacts with positive and small γ (Fig. 11(b,c)) the rear part of the particle scoops the target material in the back part of the indentation, which is visualized by the sharp rear tip of the crater. When γ is more positive (Fig. 11(d)), the positive moment on the particle is small and hence its rotation rate is not sufficient to enable scooping. By comparison to Fig. 10 we can notice that the rise in the shear energy corresponds to sharp rear tip of the formed crater. This constitute additional confirmation to the hypothesis that scooping action is responsible to increase in the shear energy.

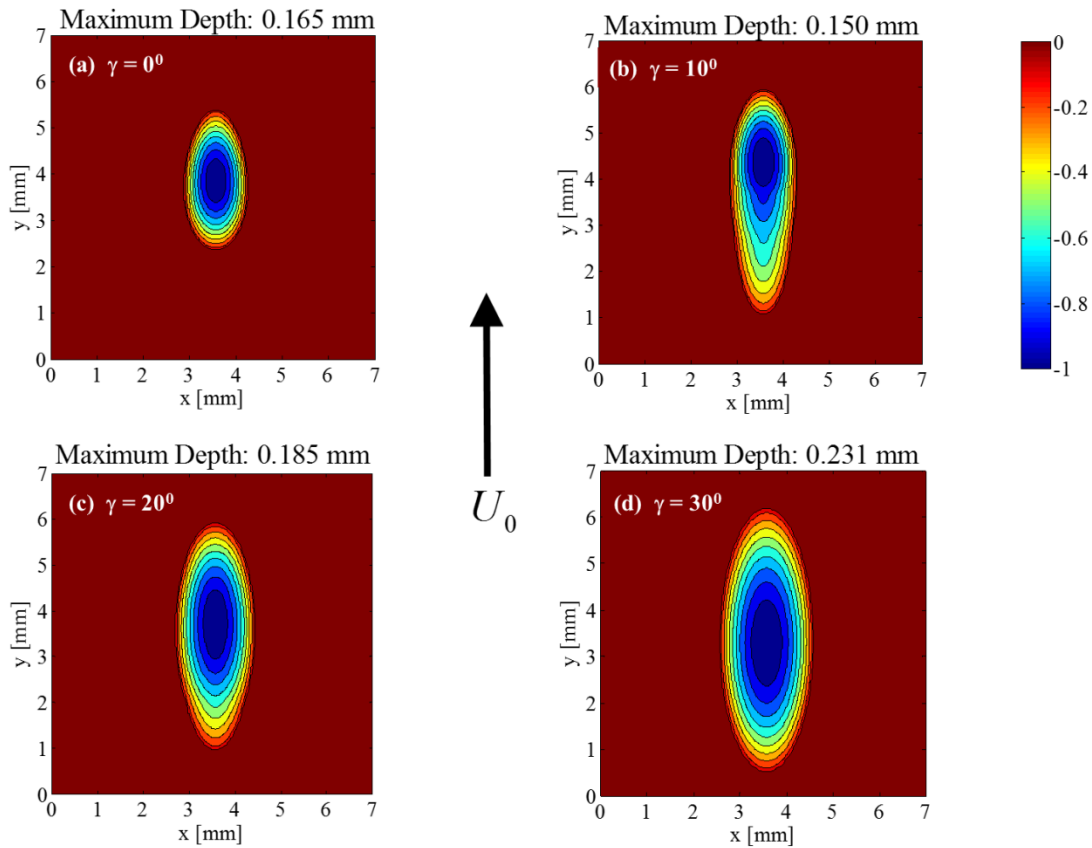


Fig. 11. Crater depth contours for the case of backward rotation $\omega_0 > 0$. Particle shape factor is $\psi = 0.7$. Impingement angle is 30° . The deviation from the standard rake angle is (a) $\gamma = 0^\circ$, (b) $\gamma = 10^\circ$, (c) $\gamma = 20^\circ$, (d) $\gamma = 30^\circ$. Colors represent the normalized depth z/z_{max} of the indentation.

8. Conclusions

- (i) A numerical model for impact of rigid particle with ductile target material was developed. The model consists 3-dimensional analysis, solving the 6 particle momentum equations and can produce with arbitrary shape particle.
- (ii) The model was validated by experimental results of Sundararajan & Shewmon [4][5] for spherical particles. The model showed good agreement with the experimental data of both indentation volume and particle energy loss.
- (iii) A study on the effect of particle shape and initial angular velocity on the erosion mechanism was conducted by simulating ellipsoid particles impact. The parameter, which was chosen to be representative of the erosion rate, is the shear energy per unit area due to its major role in the material removal process.
- (iv) The results showed a peak in the shear energy at low impingement angles (typically under 25^0) for sharp particles with initial positive rotation. This peak is related to the scooping action of the particle, i.e. the particle perform backward rotation during its movement in the target material and exit with its leading tip facing upward, while shearing the target material with its bottom surface.
- (v) In contradiction to the works of Hutchings [3] on square plates impact, ellipsoid particles usually attains backward spin during the impact. The difference behavior is due to the effect of the rhomboid sharp front tip, which does not exist in ellipsoid particles.
- (vi) The scooping mechanism can be related to the extra erosion rate of sharp particles with initial backward rotation that was reported by Deng et al. [24].
- (vii) The inclination of scooping mechanism to exist in small to intermediate impingement angles can also explain the typical erosion rate versus impingement angle curve, which shows peak erosion rate at small to intermediate impingement angles.
- (viii) The effect of initial particle orientation was studied and showed that scooping mechanism can occur at impingement angle of up to 40^0 , if the particle initial rake angle is larger than the standard rake angle $90^0 - \alpha$.

References

- [1] Finnie, I. (1960). Erosion of surfaces by solid particles. *Wear*, 3(2), 87-103.
- [2] Rickerby, D. G., & Macmillan, N. H. (1980). On the oblique impact of a rigid sphere against a rigid-plastic solid. *International Journal of Mechanical Sciences*, 22(8), 491-494.
- [3] Hutchings, I. M. (1977). Deformation of metal surfaces by the oblique impact of square plates. *International Journal of Mechanical Sciences*, 19(1), 45-52.
- [4] Sundararajan, G., & Shewmon, P. G. (1987). The oblique impact of a hard ball against ductile, semi-infinite target materials—experiment and analysis. *International journal of impact engineering*, 6(1), 3-22.
- [5] Sundararajan, G. (1990). The energy absorbed during the oblique impact of a hard ball against ductile target materials. *International Journal of Impact Engineering*, 9(3), 343-358.
- [6] Papini, M., & Spelt, J. K. (2000). Impact of rigid angular particles with fully-plastic targets Part I: Analysis. *International journal of mechanical sciences*, 42(5), 991-1006.
- [7] Papini, M., & Spelt, J. K. (2000). Impact of rigid angular particles with fully-plastic targets Part II: Parametric study of erosion phenomena. *International Journal of Mechanical Sciences*, 42(5), 1007-1025.
- [8] ElTobgy, M. S., Ng, E., & Elbestawi, M. A. (2005). Finite element modeling of erosive wear. *International Journal of Machine Tools and Manufacture*, 45(11), 1337-1346.
- [9] Wang, Y. F., & Yang, Z. G. (2008). Finite element model of erosive wear on ductile and brittle materials. *Wear*, 265(5), 871-878.
- [10] Liu, Z. G., Wan, S., Nguyen, V. B., & Zhang, Y. W. (2014). A numerical study on the effect of particle shape on the erosion of ductile materials. *Wear*, 313(1), 135-142.
- [11] Azimian, M., Schmitt, P., & Bart, H. J. (2015). Numerical investigation of single and multi-impacts of angular particles on ductile surfaces. *Wear*, 342, 252-261.
- [12] Johnson, G. R., & Cook, W. H. (1983, April). A constitutive model and data for metals subjected to large strains, high strain rates and high temperatures. In *Proceedings of the 7th International Symposium on Ballistics* (Vol. 21, pp. 541-547).
- [13] Johnson, G. R., & Cook, W. H. (1985). Fracture characteristics of three metals subjected to various strains, strain rates, temperatures and pressures. *Engineering fracture mechanics*, 21(1), 31-48.

- [14] Takaffoli, M., & Papini, M. (2012). Material deformation and removal due to single particle impacts on ductile materials using smoothed particle hydrodynamics. *Wear*, 274, 50-59.
- [15] Dong, X. W., Liu, G. R., Li, Z., & Zeng, W. (2016). A smoothed particle hydrodynamics (SPH) model for simulating surface erosion by impacts of foreign particles. *Tribology International*, 95, 267-278.
- [16] Sheldon, G. L., & Kanhere, A. (1972). An investigation of impingement erosion using single particles. *Wear*, 21(1), 195-209.
- [17] Finnie, I., & McFadden, D. H. (1978). On the velocity dependence of the erosion of ductile metals by solid particles at low angles of incidence. *Wear*, 48(1), 181-190.
- [18] Hutchings, I. M. (1981). A model for the erosion of metals by spherical particles at normal incidence. *Wear*, 70(3), 269-281.
- [19] Islam, M. A., & Farhat, Z. N. (2014). Effect of impact angle and velocity on erosion of API X42 pipeline steel under high abrasive feed rate. *Wear*, 311(1), 180-190.
- [20] Oka, Y. I., Okamura, K., & Yoshida, T. (2005). Practical estimation of erosion damage caused by solid particle impact: Part 1: Effects of impact parameters on a predictive equation. *Wear*, 259(1), 95-101.
- [21] Neilson, J. H., & Gilchrist, A. (1968). Erosion by a stream of solid particles. *Wear*, 11(2), 111-122.
- [22] Finnie, I., Stevick, G. R., & Ridgely, J. R. (1992). The influence of impingement angle on the erosion of ductile metals by angular abrasive particles. *Wear*, 152(1), 91-98.
- [23] Oka, Y. I., Ohnogi, H., Hosokawa, T., & Matsumura, M. (1997). The impact angle dependence of erosion damage caused by solid particle impact. *Wear*, 203, 573-579.
- [24] Deng, T., Bingley, M. S., & Bradley, M. S. (2004). The influence of particle rotation on the solid particle erosion rate of metals. *Wear*, 256(11), 1037-1049.
- [25] Desale, G. R., Gandhi, B. K., & Jain, S. C. (2006). Effect of erodent properties on erosion wear of ductile type materials. *Wear*, 261(7), 914-921.
- [26] Oka, Y. I., & Nagahashi, K. (2003). Measurements of plastic strain around indentations caused by the impact of round and angular particles, and the origin of erosion. *Wear*, 254(12), 1267-1275.
- [27] Arabnejad, H., Mansouri, A., Shirazi, S. A., & McLaury, B. S. (2015). Development of mechanistic erosion equation for solid particles. *Wear*, 332, 1044-1050.

- [28] Hutchings, I. M., & Winter, R. E. (1974). Particle erosion of ductile metals: a mechanism of material removal. *Wear*, 27(1), 121-128.
- [29] Levy, A. V. (1986). The platelet mechanism of erosion of ductile metals. *Wear*, 108(1), 1-21.
- [30] Sundararajan, G. (1991). A comprehensive model for the solid particle erosion of ductile materials. *Wear*, 149(1-2), 111-127.
- [31] Winter, R. E., & Hutchings, I. M. (1975). The role of adiabatic shear in solid particle erosion. *Wear*, 34(2), 141-148.
- [32] Lindroos, M., Ratia, V., Apostol, M., Valtonen, K., Laukkanen, A., Molnar, W., & Kuokkala, V. T. (2015). The effect of impact conditions on the wear and deformation behavior of wear resistant steels. *Wear*, 328, 197-205.
- [33] Johnson, W. (1972). *Impact strength of materials*. London: Edward Arnold.
- [34] Johnson, K. L. (1987). *Contact mechanics*. Cambridge university press.
- [35] Brach, R. M. (1988). Impact dynamics with applications to solid particle erosion. *International journal of impact engineering*, 7(1), 37-53.